Opto-Electronic Science

Review

2022, Vol. 1, No. 4

DOI: 10.29026/oes.2022.210004

Applications of optically and electrically driven nanoscale bowtie antennas

Zhongjun Jiang†, Yingjian Liu† and Liang Wang*

Optical antennas play an important role in optical field manipulation. Among them, nanoscale bowtie antennas have been extensively studied for its high confinement and enhancement. In this mini-review, we start with a brief introduction of bowtie antennas and underlying physics. Then we review the applications with respect to optically and electrically excited nanoscale bowtie antennas. Optically driven bowtie antennas enable a set of optical applications such as near-field imaging/trapping, nonlinear response, nanolithography, photon generation and detection. Finally, we put emphasis on the principle and applications of electrically driven bowtie antennas, an emerging method of generating ultrafast and broadband tunable nanosources. In a word, nanoscale bowtie antennas still have great potential research value to explore.

Keywords: bowtie antenna; near-field imaging; nanolithography; nonlinear; nanolaser; inelastic tunneling

Jiang ZJ, Liu YJ, Wang L. Applications of optically and electrically driven nanoscale bowtie antennas. *Opto-Electron Sci* **1**, 210004 (2022).

Introduction

It has been a long time for researchers to explore methods to overcome the diffraction limit. Although light can be squeezed through a sub-wavelength hole[1] leading to lateral resolution on the order of the hole size, its transmission is very limited based on Bethe's law[2]. However, it has been noticed that bowtie antennas (Fig. 1(a)) enable simultaneous high resolution and enhanced transmission[3], which is suitable for near-field imaging techniques such as scanning near-field optical microscopy (SNOM) and near field lithography. This phenomenon can be simply explained as follows. The two arms of the bowtie antenna have large surface areas to efficiently collect the incident radiation. Incident light polarized along the gap of the bowtie antenna generates surface currents to carry surface charge to the sharp tips (Fig. 1(c)). The opposite oscillating surface charges at the tips behave like an oscillating electric dipole which radiates light through the aperture. Therefore, light with proper polarization can pass through the bowtie antenna without experiencing much intensity decay. The transmitted light is confined underneath the nanoscale gap region offering an optical resolution far beyond the diffraction limit.

In a more general way, bowtie antennas (hereafter, bowties) acting as optical antennas, receive and emit radiation as they do in the microwave regime[5,6]. It means that bowties, regardless of whether it is apertured (Fig. 1(a)) or gaped (Fig. 1(b)), can convert an external electromagnetic field into a confined energy[7,8], and vice versa. Field confinement and enhancement presented in the gap region, thus can be utilized to achieve a variety of optical applications.

Since the early 2000s, bowtie structures have been used as electrodes in molecular engineering[9] and applied

Department of Optics and Optical Engineering, University of Science and Technology of China, Hefei 230026, China.

†These authors contributed equally to this work.

*Correspondence: L Wang, E-mail: lwang121@ustc.edu.cn

Received: 8 June 2021; Accepted: 4 November 2021; Published online: 20 April 2022

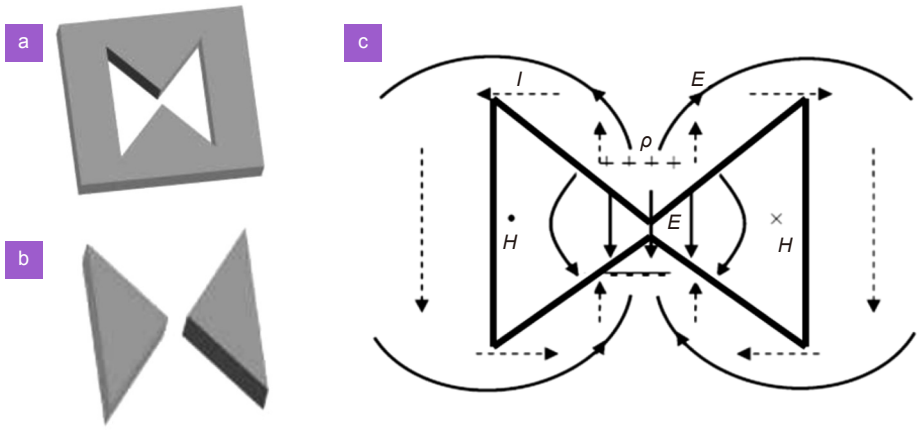

Fig. 1 | Bowtie apertured (**a**) and gaped (**b**) antennas. (**c**) Induced surface charges and electric dipole when incident electric field polarizes along the tips. Figure reproduced with permission from: (a-b) ref.[4], Copyright 2006 American Chemical Society.

in molecular junctions to investigate electroluminescence[10], and high-conductivity[11,12]. Thanks to the development of nanofabrication, bowties in nanometer scale dimensions[13–15] brought about widespread optical applications. In 2006, sub-diffraction nanoscale lithography with bowties[4,16] have been demonstrated. Nanolaser based on bowties array was achieved by exciting dye molecules centered in the gap, in 2012[17]. In 2018, enhanced absorption via bowtie arrays in 2D black phosphorus was achieved based on the high transmission of the antenna and a perfect polarization selection ratio is observed[18]. Recently, nanoscale bowties were reported to be excited by not only external light, but also electricity[19], showing its advantages in high intensity and ultrafast optical response. As we will show, the last decades have witnessed the booming development of bowties under the optical or electrical excitation.

This paper aims to review applications of optically and electrically driven nanoscale bowties. Since rapid advances have been made in this area, it is difficult to cover all the related references in this review. Nonetheless, we hope the present review arouse interest among the researchers in this subject.

Optically driven nanoscale bowties

Due to the high enhancement and confinement of bowties, strong electric field localizations[20–22] (hot spots) are presented in the gap. These properties promise bowties broad applications ranging from light transmitting, frequency doubling/tripling, focusing, and generation to detection. In this section, we present an overview of the applications of optically excited bowties.

Nanoimaging and nanotrapping

As mentioned before, bowties exhibit highly enhanced fields under the illumination of light. The consequently enhanced light transmission guarantees a set of nanotechnologies such as nanoimaging and trapping.

Near-field imaging techniques, e.g., SNOM, utilizes evanescent waves to generate sub-diffraction-limit resolution. As the evanescent components decay exponentially, SNOM uses a tapered fiber[23] as a probe and needs to work close to the sample surface. Even in this situation, the light coupling efficiency is severely limited because of the poor transmission of the fiber tip. Therefore subwavelength apertures are usually constructed on the tip apex to boost the light collection. Bowtie apetures[3,24] are favored over other apertures owing to its giant light field enhancement[13]. Wang et al.[3] fabricated metallic bowtie and square apertures on the quartz wafer, and compared their far-field transmission (Fig. 2(a)). Results indicated that the transmission was enhanced exceeding one order of magnitude from bowtie apertures than the squared ones with the same opening areas. Bowtie apertures were then milled on the SNOM probe (Fig. 2(b)), showing a seven times higher near-field measurement counts than the regular aperture probe (Fig. 2(c)).

Strong energy confinement with a high optical gradient provided by bowties also promises applications in optical trapping[25–27]. Using a bowtie plasmonic aperture that was patterned on a tapered metal-coated fiber[25], 50 nm polystyrene beads were successfully captured, demonstrating the feasibility of nanoparticle trapping. Notably, 4-nm quantum dot was experimentally reported to be trapped in a deep potential well (Fig. 2(e)) using the three-dimensional tapered 5-nm-gap bowtie

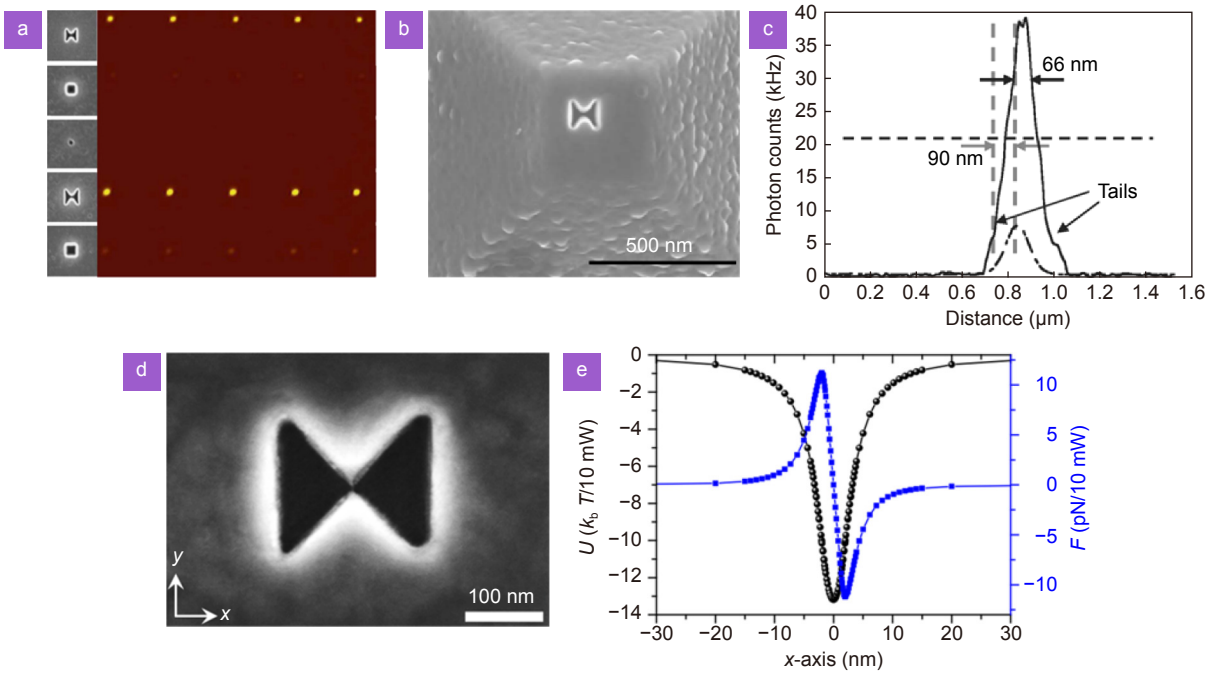

Fig. 2 | Near-field imaging and trapping using (apertured) bowties. (**a**) Transmission through the subwavelength apertures. Bowtie apertures show much enhanced transmission. Left: different apertures. Right: far-field transmission measurements. (**b**) Bowtie apertures fabricated on the SNOM probe. (**c**) Line profiles of SNOM images using bowtie (solid line) and square (dashed line) aperture probes. (**d**) 5-nm-gap bowtie apertures. (**e**) Optical potentials *U* and the corresponding optical forces *F* along the *x*-axis. Figure reproduced with permission from: (a–c) ref.[3], Copyright 2007 AIP Publishing; (d–e) ref.[27], Copyright 2018 the author(s), under a Creative Commons Attribution 4.0 International License.

aperture antenna (Fig. 2(d)).

Nonlinear response

Typically optical antennas work in the linear regime for weak excitation fields. In other words, the nonlinearity is negligible in most cases. The nonlinear conversion efficiency, however, can be resonantly enhanced by localized surface plasmons (LSPs)[28] when appropriate size and shape of the nanoantenna are introduced. As a consequence, new interesting phenomena arise, such as frequency conversion, switching, and modulation[29].

Bowties exhibit power enhancement factors larger than 40 dB[30], which is beneficial to second or even higher order harmonics generation[31]. As shown in Fig. 3(a), large arrays of antennas are often used to boost nonlinear conversion efficiency[32–34]. Nevertheless, Hanke et al.[35] observed that third harmonic (visible light) was emitted by using individual bowtie antenna excited resonantly with few-cycle femtosecond laser (~0.6 MW/cm^2) in the near infrared. Though the second-order harmonic generation is partially constrained by the symmetry condition, it was also observed in the emission spectra with a small peak (Fig. 3(b)). It has been reported[30] that bowties are even capable of lowering the pulsed femtosecond laser intensities (from 10^{13} MW/cm^2 to 10^{11} MW/cm^2 level) that are required to produce coherent extreme-ultraviolet (EUV) light through the nonlinear conversion process. High harmonics up to 17th were observed.

Two-photon photoluminescence (TPPL) can also occur because of high local fields at LSP resonance and shows $E^4_{\rm local}$ dependence on the local *E* fields[15] (Fig. 3(c)).

Nanolithography

The development of modern information technologies makes a request of advanced nano-manufacturing tools. As we will see, great success has been achieved in nanolithography via bowties in the last decades. Bowties are capable of focusing the incident ultra-violet (UV) light into a small spot, showing remarkable advantages over traditional optical lithography, e.g., deep UV and extremely UV lithography, for its low cost and competitive resolution. In 2006 Wang et al.[4] fabricated apertured bowties by focused ion beam (FIB) on a 150 nm thick aluminum film (Fig. 4(a)). Under the illumination of 355 nm light, 40×50 nm lithography resolution was experimentally reported, as shown in Fig. 4(b). Higher resolution becomes more noticeable by fabricating an ultrasmall gap between the antenna tips with the back-side milling method[36]. Another nice experiment was conducted by Sundaramurthy et al.[16] in the same year. They

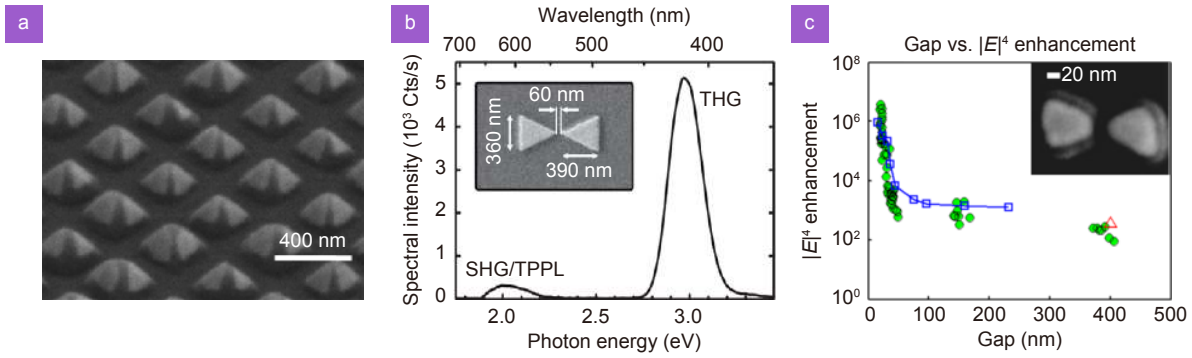

Fig. 3 | Nonlinear response in bowties. (**a**) Three-dimensional (3D) gold bowties array. (**b**) Nonlinear emission spectrum from a single bowtie (inset). (**c**) Spectrum of generated high harmonics from 2D bowties array (inset). (**d**) Experimental (TPPL, circles) and theoretical (field enhancement, squares) results versus bowtie gap size. Inset shows a bowtie with a 22 nm gap. Figure reproduced with permission from: (a) ref.[32], American Chemical Society; (b) ref.[35], under a Creative Commons Attribution 3.0 License; (c) ref.[15], American Physical Society.

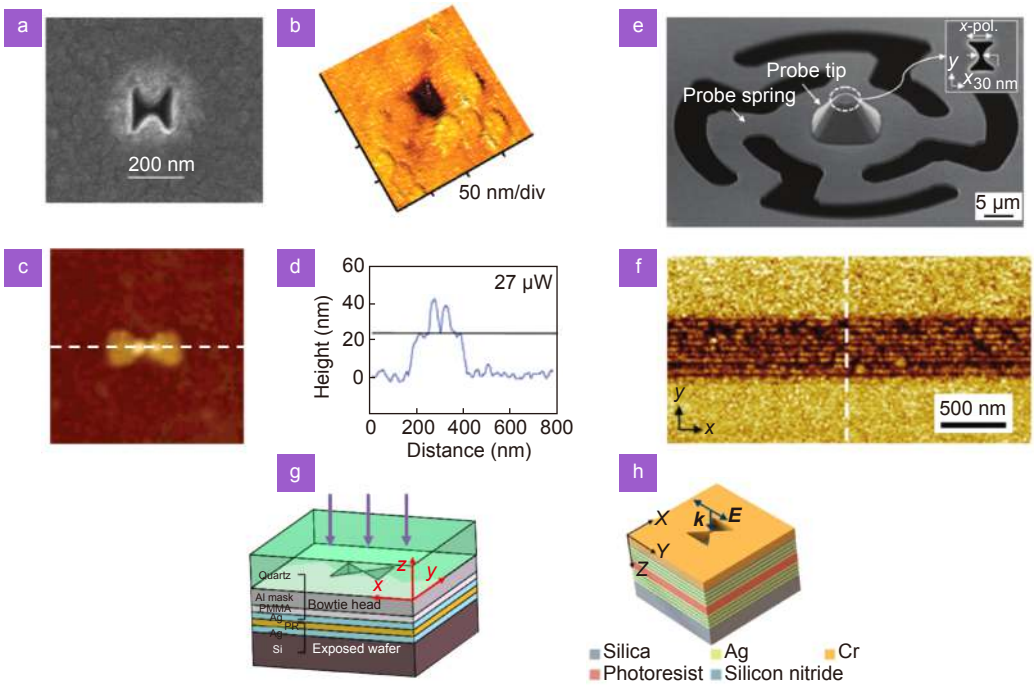

Fig. 4 | Nanolithography using bowties. (**a**) Bowtie apertures with a 30 nm gap. (**b**) AFM image of 40 nm × 50 nm lithography hole. (**c**–**d**) AFM image (c) and cross section (d) along the nanoantenna axis of bowties exposed at 25 μW laser power. Feature size of ~30 nm for each of the resist pillars was measured. (**e**) SEM image of the fabricated circular contact probe. (**f**) AFM image of a 22-nm half pitch resolution line array pattern. (**g**–**h**) Bowtie nanolithography combined with metal-insulator-metal (g) and hyperbolic metamaterials (h). Figure reproduced with permission from: (a, b) ref.[4], Copyright 2016 American Chemical Society; (c, d) ref.[16], American Chemical Society; (e, f) ref.[37], Copyright 2012 John Wiley and Sons; (g) ref.[38], Copyright 2019 Optical Society of America; (h) ref.[41], IOP Publishing.

demonstrated that by utilizing optically resonant metallic bowties, the production of polymer resist nanostructures <30 nm in diameter was achieved at a longer wavelength of 800 nm via the two-photon polymerization (TPP) effect (Fig. 4(c) and 4(d). Researchers[37] from Yonsei University has shown that by using a contact probe made of bowtie aperture antennas (Fig. 4(e)) illuminated by a 405 nm wavelength laser light, high-density line array patterns were recorded with a half pitch up to 22 nm (Fig. 4(f)). Further, the line edge roughness was decreased down to be ~ 17 nm by optimizing the developing process. This work implies bowties-based nanolithography has a great potential for practical applications.

While sub-diffraction resolution (<20 nm)[36] can be achieved by using bowties, nearly all the aforementioned results suffer from a small depth of focus (DOF: <10 nm), which poses challenges for industrial production.

Such a problem is alleviated by combining bowtie antennas with metamaterials, such as silver superlens/reflectors[38–40] (Fig. 4(g), DOF: ~30 nm) and hyperbolic metamaterials[41] (Fig. 4(h), DOF: ~100 nm). However, the DOF has to be larger than 100 nm to realize convenient and reliable pattern transferring. This has to be addressed before taking bowtie nanolithography a step closer to widespread applications.

Nanosources

Miniaturized photon sources are essential elements for all-optical circuits and nanoscale biosensors. One way of achieving lasing from nanoscale resonators is to utilize LSPs excited in metal nano-particles. A bowtie-shaped metallic resonator are well suited for this purpose as it can provide high Purcell factor thanks to the high confinement, therefore, the ultra-small effective mode volume[42]. In addition, the threshold condition for lasing can be satisfied at room temperature near LSP resonance wavelengths. Shown in Fig. 5(a), Jae Yong Suh et al.[17] demonstrated that three-dimensional (3D) nano-bowties array coupled with a gain medium (IR-140 dye in polyurethane) can generate coherent and directional light emission (Fig. 5(b) and 5(c)). With a mode volume smaller than $0.001(\lambda/2n)^3$ (λ, the wavelength and n, the effective refractive index), room temperature optically pumped lasing at 873 nm with a threshold pump pulse fluence of 0.4 mJ/cm^2 was observed.

Bowties also show great potential for high-contrast selection of single nanoemitters[43]. Kinkhabwala et al.[43] observed enhancements of a single molecule's fluorescence up to a factor of 1340 by using fluorescent molecules coated bowties. They attributed this to the result of greatly enhanced absorption and an increased radiative emission rate due to the presence of bowties.

Moving towards the infrared band, silicon carbide bowties (Fig. 5(d)) can serve as a thermal emitter with a narrowband (10 cm^{-1}) spectrum[44] (Fig. 5(f)), which is suitable for novel applications such as non-dispersive infrared sensing and molecular spectroscopy. The thermal emission spectrum show a clear dependence on the bowtie gap size, indicating that a tunable thermal emitter is achievable. Numerical simulations (Fig. 5(e)) and near-field optical characterization shade light on the physical nature of the resonances in the thermal emission spectra.

Photodetectors

The strong plasmonic enhancement between the bowtie tips results in an enhanced in-plane electric fields interaction with two-dimensional (2D) materials, leading to an efficiently absorbed external light. Consequently, bowties have been utilized to enhance the responsivity of photodetectors. For example, Ma et al.[45] reported that a bowtie-enhanced graphene waveguide photodetector possesses a high external responsivity of 0.5 A/W and a fast frequency response up to at least 110 GHz (Fig. 6(a–c)). As a validation of optical communication, 100 Gbit/s data reception of two-level OOK and four-level PAM-4 intensity encoded signals was successfully demonstrated at C-band (Fig. 6(d)). Venuthurumilli et al.[18] also demonstrated a near infrared photodetector using black phosphorus embellished by bowties, as shown in Fig. 6(e) and 6(g). High photocurrent (an enhancement of 70% in comparison to the device without bowties, Fig. 6(f)) or polarization sensitivity (8.7, Fig. 6(h)) can be achieved with proper bowtie designs and orientations.

Electrically driven nanoscale bowties

Nanoantennas can be excited by not only the external light, but also the bias voltages. They function as an emerging optical nano-source[46–49] via the inelastic electron tunneling (IET) process. Related researches can date back to 1976 in biased metal-insulator-metal junctions[50], and lately, in scanning tunneling microscope (STM) systems[51–53]. Electrically driven antennas bridge electrical and optical circuits at the nanoscale and constitute a vibrant sub-field of nano-photonics.

We also notice that bowtie-shaped metallic structures are widely used in molecule engineering as electrical leads, to exploit charge transport at the level of single molecules[54]. Strictly speaking, however, these devices can hardly be regarded as 'antennas' due to the lack of related functions. Therefore in this section, we will devote special attention to light emission from electrically excited bowtie antennas, including the principles, fabrication, characterizations and future directions.

Underlying mechanisms

A tunnel junction can be made of a thin insulating layer (usually the air or, here, oxide) sandwiched between the two conducting materials (e.g., here, Al and Au), as illustrated in Fig. 7(a). When voltages are applied, electrons

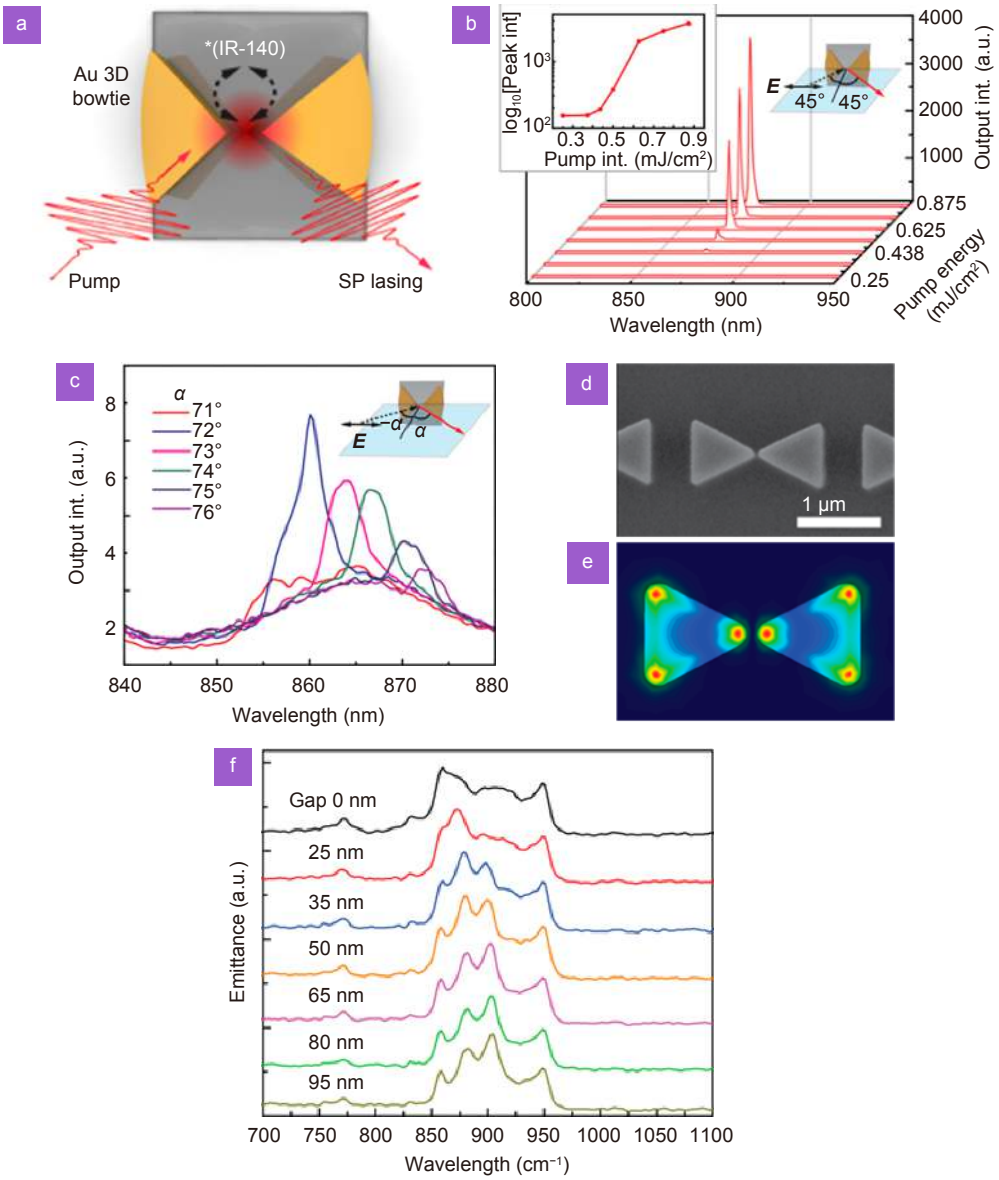

Fig. 5 | Bowtie based nanosources. (**a**) Schematic of 3D bowtie plasmonic lasers. (**b**) Evolution of lasing spectra from 3D Au bowties under pump polarization parallel to the tip axis. Inset shows emission intensity versus pump pulse energy density plotted on a semilogarithmic scale. (**c**) Directional SP out-coupling emission. (**d**) Bowties with a small gap. (**e**) Simulated near-field patterns of one of resonant modes in bowties. (**f**) Thermal emission spectrum under different bowtie gap sizes. Figure reproduced with permission from: (a–c) ref.[17], Copyright 2012 American Chemical Society; (d–f) ref.[44], Copyright 2017 the author(s), under the ACS AuthorChoice via CC-BY-NC-ND Usage Agreement.

could tunnel through the barrier inelastically and give rise to an energy transfer in the form of (localized or propagated) surface plasmons (Fig. 7(b)). Light can be emitted by the radiative decay or scattering of surface plasmons[55]. Since the tunneling process happens at a time scale of femtoseconds[56,57], it enables electrically driven antennas to be operated as an ultrafast optical source.

A typical signature of IET is that the cut-off frequency v in electroluminescence spectrum is related to the applied bias voltage $V_{\rm bias}$ (Fig. 8(c)), also known as the quantum limit $hv \leqslant {\rm e}\,|V_{\rm bias}|$ in which h the Planck's constant and e the electron charge. Interestingly, an alternative mechanism that might explain the light emission from tunnel junctions is resulted from hot-electron decay[58], where the energies of emitted photons are beyond the quantum limit. Our focus is concentrated on the IET process. IET can be theoretically described as an energy-loss model, current fluctuations model and spontaneous emission model. We refer the interested readers to the review[59] for more mathematic details. Here, we briefly give a physical picture behind light emission from

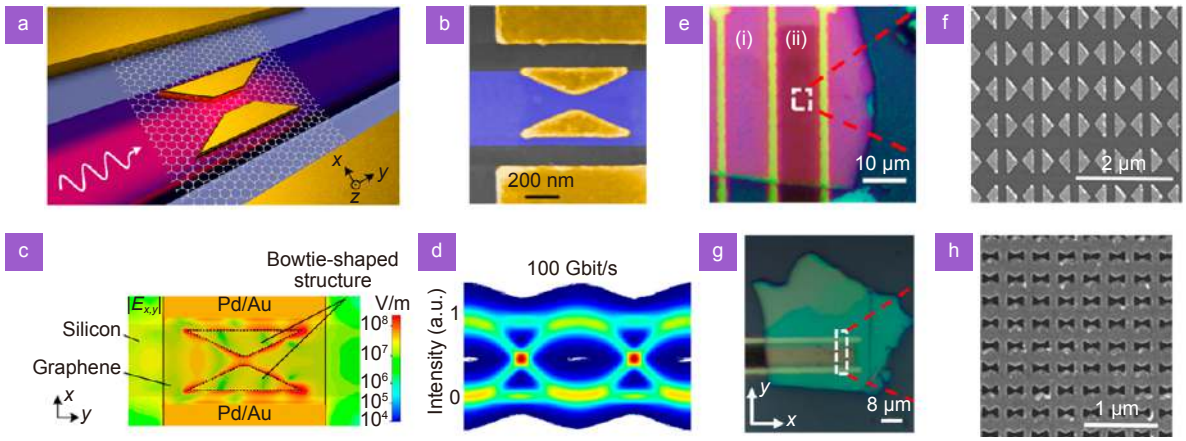

Fig. 6 | 2D materials photodetectors based on bowties. (**a**) Schematic and (**b**) SEM image of the plasmonically enhanced graphene photodetector. (**c**) The magnitude of in-plane electric fields. Strong plasmonic field enhancements in the gap were observed. (**d**) Eye diagram of 100 Gbit/s OOK optical signals. (**e**) Optical and (**f**) SEM image of bowtie gap antennas for high responsivity detectors. (**g**) Optical and (**h**) SEM image of bowtie aperture antennas for high polarization. Figure reproduced with permission from: (a–d) ref.[45], Copyright 2019 The Author(s), under the ACS AuthorChoice Usage Agreement; (e–h) ref.[18], Copyright 2018 American Chemical Society.

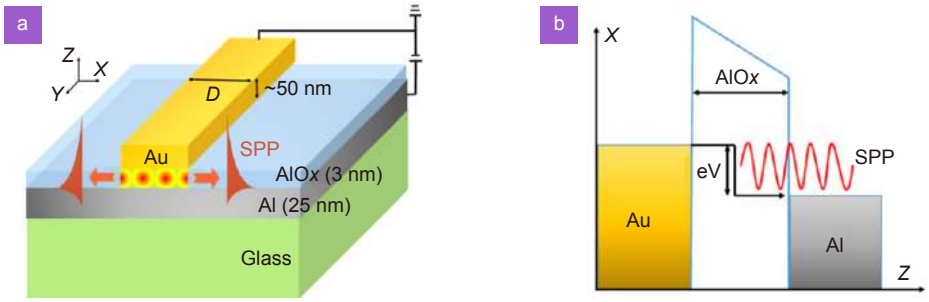

Fig. 7 | Surface plasmons mediated via the IET process. (**a**) Schematic of the Al-AlO$_x$-Au tunnel junction. (**b**) Energy level diagram of the IET process. (**c**) Bias dependent emission spectra. Emitted photons with cut-off frequencies can be seen. Figure reproduced with permission from ref.[49], under a Creative Commons Attribution 4.0 International License.

electrically driven antennas, as follows.

The (detectable) electron-to-photon conversion efficiency, or, the external quantum efficiency (EQE) driven by IET can be described as

$$\mathrm{EQE} = \eta_0^{\mathrm{IET}} \frac{P_{\mathrm{total}}}{P_0} \frac{P_{\mathrm{rad}}}{P_{\mathrm{total}}}, \tag{1}$$

where η_0^{IET} is the source efficiency of IET in vacuum (in the order of 10^{-6} level at visible frequencies with a modest dependence on the details of the barriers[59]), P_0 is the power emitted by a dipole in free space, P_{total} is the total power dissipated (not directly to photon emission but often in the form of other types of optical modes, such as LSP modes) by a dipole in an arbitrary environment and P_{rad} is the radiated power. The key is that, the ratio of P_0 and P_{total} is deeply connected to the quantity, the partial local density of the optical states (LDOS) ρ_{p}, that is[59]

$$\frac{P_{\mathrm{total}}}{P_0} = \frac{\rho_{\mathrm{p}}}{\rho_0}, \tag{2}$$

where ρ_0 is the vacuum LDOS. The radiation efficiency η_{rad} is defined as $P_{\mathrm{rad}}/P_{\mathrm{total}}$. Both the LDOS and radiation efficiency (Fig. 8(d) and 8(e)) are profoundly influenced by the geometries of bowties (say, for example, the bowtie width, height and angle shown in Fig. 8(a)). This demonstrates the practicality of tunable nano-sources based on bowtie junctions. Although the LDOS and η_{rad} cannot be analytically expressed except a few kinds of geometries, Eq. (2) points out a viable way of estimating EQE by numerical simulations using the Green's function[60].

Fabrication of bowtie antenna based tunnel junctions

Tunnel junctions can be classified into two categories, namely, the vertical (for example, shown in Fig. 7(a)) and lateral junctions (Fig. 8(a)), in terms of their orientations relative to the substrate. As for the vertical junctions, they are formed due to the nature of oxidation. When it comes to the lateral counterpart, while the

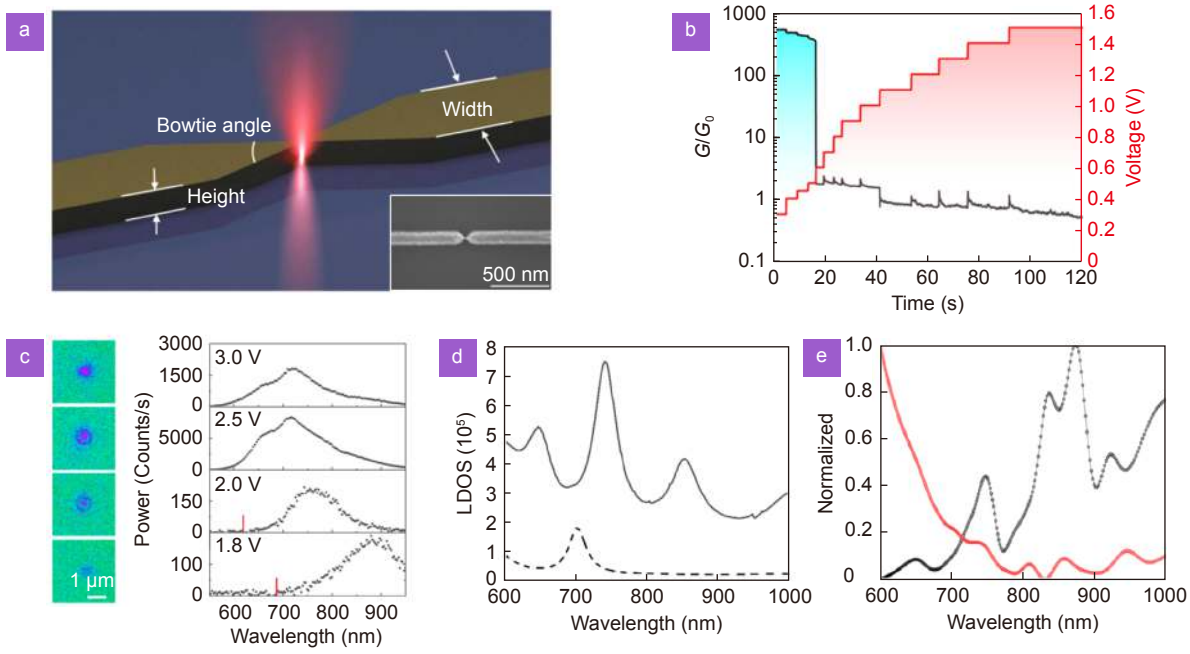

Fig. 8 | Light emission from bowtie antenna based tunnel junctions. (**a**) Lateral tunnel junctions made by bowtie gap-antennas. Inset shows that the bowtie antennas are connected before the electro-migration process. (**b**) Time evolution of normalized conductance (G/G_0). (**c**) Light emission spectra. Left column: images captured under different biases. Right column: spectral evolution under different bias. (**d**) Enhanced LDOS in the order of 10^5. Solid line: bowties case. Dashed lines: nanowire case. (**e**) Wavelength dependent normalized LDOS (red) and radiation efficiency (black). They both contribute to the ultimate emission spectrum. Figure reproduced with permission from: (a–d) ref.[19], Copyright 2019 American Chemical Society; (e) ref.[64], Copyright 2020 Optical Society of America.

ultra-small (sub 1 nm) gap is hard to fabricate using currently available nanopatterning methods[61], electro-migration[62,63] is a good choice to generate bowtie gap-antenna tunnel junctions. This process[19,64] starts with the patterning of weakly-bridged (the smallest linewidth is 10 nm) bowties by electron beam lithography, followed by supplying a gradually-increasing bias voltages till the conductance G of the antennas drops well below the quantum conductance[65] $G_0 = 2e^2/h$ (shown in Fig. 8(b)). It is at this stage that a tiny gap appears. Our group has demonstrated a 0.6 nm gap bowtie antenna[19] obtained by a well-controlled electro-migration process.

Characterizations

Thanks to the well-designed bowtie gap-antenna tunnel junctions, we have achieved a broadband optical nano-source driven by IET (see Fig. 8(c)) with peak emission power of 1.4 nW[19], which is two orders of magnitude higher than previous results (see Table 1). The EQE is then calculated to be $(1.1 \pm 0.2) \times 10^{-4}$. It is not hard to understand either from the point view of enhanced LDOS (see Fig. 8(d)), or enhanced Purcell factors[66] due to the small mode volume in bowties. Further, bowtie-shaped structures also function as 'antennas', providing a high radiation efficiency (of course, at specific wavelengths). Accordingly, the emission spectrum can be tuned by engineering LDOS and radiation efficiency (Fig. 8(e)), as explained in *Underlying Mechanisms*. Wang et al. recently have used an approximate model[64] to analytically calculate the resonant peaks in the emission spectra of electrically driven bowties, showing a good agreement with the experimental results.

Future directions

Higher efficiencies[48] are continually pursued by researchers. While EQE roughly shows a dependence on the width d of tunnel gap (d^{-1})[59], however, d cannot be unlimited shortened because quantum mechanics dominates then. The operating speed and footprint may be priority depending on applications. In recent years, two-dimensional materials integrated tunnel devices[67,68] attract much attention and remain to be further explored. Directional control of electrically excited sources[69–71] via IET is also of particular interest by using properly designed antenna architectures.

Summary

Owing to the field confinement and enhancement, nanoscale bowties can be a good fit for a variety of applications

Table 1 | Comparison on the performance of tunnel junctions

References	Width of the tunnel gap	Tunnel current	Type of the tunnel junction	Output power	EQE	Measuring tool
ref.[46]	1.3 nm	~2 nA @ 1.5 V	Au-air-Au	/	3×10^{-4}	EMCCD
ref.[47]	2.0 nm	~10 nA	Al-AlO_x–Au	/	/	EMCCD
ref.[48]	1.5 nm	~25 nA @ 2.5 V	Ag-PVP-Ag	30 pW	2×10^{-3}	EMCCD
ref.[69]	1.1 nm	~10 nA @ 1.5 V	Au-air-Au	/	$\sim1\times10^{-5}$	EMCCD
ref.[72]	30 nm	~100 nA @15 V	Au-air-Au	/	/	EMCCD
ref.[19]	0.6 nm	~5 μA @ 2.5 V	Au-air-Au	1.4 nW	$\sim1.1\times10^{-4}$	sCMOS

EMCCD: electron-multiplying charge-coupled device sCMOS: scientific complementary metal–oxide–semiconductor

such as near-field imaging, nanotrapping, nanolithography, nano-sources and photodetectors, etc. This review presents the applications of nanoscale bowties excited by photons and electrons. Bowties can be used for bridging electronic and photonic components on a same chip, thus possessing great potential in high-density optical storage and on-chip wireless communication. Nanoscale bowties may meet great challenges but could also lead photonic chip researches to a new step in the future.

References

1. Synge EH. XXXVIII. A suggested method for extending microscopic resolution into the ultra-microscopic region. *London, Edinburgh, Dublin Philos Mag J Sci* **6**, 356–362 (1928).
2. Bethe HA. Theory of diffraction by small holes. *Phys Rev* **66**, 163–182 (1944).
3. Wang L, Xu XF. High transmission nanoscale bowtie-shaped aperture probe for near-field optical imaging. *Appl Phys Lett* **90**, 261105 (2007).
4. Wang L, Uppuluri SM, Jin EX, Xu XF. Nanolithography using high transmission nanoscale bowtie apertures. *Nano Lett* **6**, 361–364 (2006).
5. Balanis CA. *Antenna Theory: Analysis and Design* (Harper & Row, New York, 1982).
6. Grober RD, Schoelkopf RJ, Prober DE. Optical antenna: towards a unity efficiency near-field optical probe. *Appl Phys Lett* **70**, 1354–1356 (1997).
7. Krasnok AE, Maksymov IS, Denisyuk AI, Belov PA, Miroshnichenko AE et al. Optical nanoantennas. *Phys-Usp* **56**, 539–564 (2013).
8. Bharadwaj P, Deutsch B, Novotny L. Optical antennas. *Adv Opt Photonics* **1**, 438–483 (2009).
9. Park J, Pasupathy AN, Goldsmith JI, Chang C, Yaish Y et al. Coulomb blockade and the Kondo effect in single-atom transistors. *Nature* **417**, 722–725 (2002).
10. Huang JS, Kern J, Geisler P, Weinmann P, Kamp M et al. Mode imaging and selection in strongly coupled nanoantennas. *Nano Lett* **10**, 2105–2110 (2010).
11. Sun HT, Liu XS, Su YJ, Deng B, Peng HL et al. Dirac-cone induced gating enhancement in single-molecule field-effect transistors. *Nanoscale* **11**, 13117–13125 (2019).
12. Sun HT, Jiang ZL, Xin N, Guo XF, Hou SM et al. Efficient fabrication of stable graphene-molecule-graphene single-molecule junctions at room temperature. *Chemphyschem* **19**, 2258–2265 (2018).
13. Şendur K, Challener W. Near-field radiation of bow-tie antennas and apertures at optical frequencies. *J Microsc* **210**, 279–283 (2003).
14. Jin EX, Xu XF. Obtaining super resolution light spot using surface plasmon assisted sharp ridge nanoaperture. *Appl Phys Lett* **86**, 111106 (2005).
15. Schuck PJ, Fromm DP, Sundaramurthy A, Kino GS, Moerner WE. Improving the mismatch between light and nanoscale objects with gold bowtie nanoantennas. *Phys Rev Lett* **94**, 017402 (2005).
16. Sundaramurthy A, Schuck PJ, Conley NR, Fromm DP, Kino GS et al. Toward nanometer-scale optical photolithography: utilizing the near-field of bowtie optical nanoantennas. *Nano Lett* **6**, 355–360 (2006).
17. Suh JY, Kim CH, Zhou W, Huntington MD, Co DT et al. Plasmonic bowtie nanolaser arrays. *Nano Lett* **12**, 5769–5774 (2012).
18. Venuthurumilli PK, Ye PD, Xu XF. Plasmonic resonance enhanced polarization-sensitive photodetection by black phosphorus in near infrared. *ACS Nano* **12**, 4861–4867 (2018).
19. Qin J, Liu YJ, Luo HW, Jiang ZJ, Cai WS et al. Tunable light emission by electrically excited plasmonic antenna. *ACS Photonics* **6**, 2392–2396 (2019).
20. Dodson S, Haggui M, Bachelot R, Plain J, Li SZ et al. Optimizing electromagnetic hotspots in plasmonic bowtie nanoantennae. *J Phys Chem Lett* **4**, 496–501 (2013).
21. Chen Y, Chen YH, Chu JR, Xu XF. Bridged bowtie aperture antenna for producing an electromagnetic hot spot. *ACS Photonics* **4**, 567–575 (2017).
22. Chen Y, Chen JF, Xu XF, Chu JR. Fabrication of bowtie aperture antennas for producing sub-20 nm optical spots. *Opt Express* **23**, 9093–9099 (2015).
23. Valaskovic GA, Holton M, Morrison GH. Parameter control, characterization, and optimization in the fabrication of optical fiber near-field probes. *Appl Opt* **34**, 1215–1228 (1995).
24. Atie EM, Xie ZH, El Eter A, Salut R, Nedeljkovic D et al. Remote optical sensing on the nanometer scale with a bowtie aperture nano-antenna on a fiber tip of scanning near-field optical microscopy. *Appl Phys Lett* **106**, 151104 (2015).
25. Berthelot J, Aćimović SS, Juan ML, Kreuzer MP, Renger J et al. Three-dimensional manipulation with scanning near-field optical nanotweezers. *Nat Nanotechnol* **9**, 295–299 (2014).
26. Hameed NM, El Eter A, Grosjean T, Baida FI. Stand-Alone Three-Dimensional Optical Tweezers Based on Fibred Bowtie Nanoaperture. *IEEE Photonics Journal* **6**, 1–10 (2014).
27. Yoon SJ, Lee J, Han S, Kim CK, Ahn CW et al. Non-fluorescent nanoscopic monitoring of a single trapped nanoparticle via nonlinear point sources. *Nat Commun* **9**, 2218 (2018).
28. Kelly KL, Coronado E, Zhao LL, Schatz GC. The optical properties of metal nanoparticles: the influence of size, shape, and

dielectric environment. *J Phys Chem B* **107**, 668–677 (2003).
29. Harutyunyan H, Volpe G, Novotny L. *Nonlinear optical antennas*. Agio M, Alù A. Optical Antennas 131–143 (Cambridge University Press, New York, 2013).
30. Kim S, Jin J, Kim YJ, Park IY, Kim Y et al. High-harmonic generation by resonant plasmon field enhancement. *Nature* **453**, 757–760 (2008).
31. Suh JY, Odom TW. Nonlinear properties of nanoscale antennas. *Nano Today* **8**, 469–479 (2013).
32. Suh JY, Huntington MD, Kim CH, Zhou W, Wasielewski MR et al. Extraordinary nonlinear absorption in 3D bowtie nanoantennas. *Nano Lett* **12**, 269–274 (2012).
33. Bar-Lev D, Scheuer J. Efficient second harmonic generation using nonlinear substrates patterned by nano-antenna arrays. *Opt Express* **21**, 29165–29178 (2013).
34. Ko KD, Kumar A, Fung KH, Ambekar R, Liu GL et al. Nonlinear optical response from arrays of Au bowtie nanoantennas. *Nano Lett* **11**, 61–65 (2011).
35. Hanke T, Krauss G, Träutlein D, Wild B, Bratschitsch R et al. Efficient nonlinear light emission of single gold optical antennas driven by few-cycle near-infrared pulses. *Phys Rev Lett* **103**, 257404 (2009).
36. Chen Y, Qin J, Chen JF, Zhang L, Ma CF et al. 16 nm-resolution lithography using ultra-small-gap bowtie apertures. *Nanotechnology* **28**, 055302 (2017).
37. Kim S, Jung H, Kim Y, Jang J, Hahn JW. Resolution limit in plasmonic lithography for practical applications beyond 2x-nm half pitch. *Adv Mater* **24**, OP337–OP344 (2012).
38. Jiang ZJ, Luo HW, Guo SP, Wang L. 40 nm thick photoresist-compatible plasmonic nanolithography using a bowtie aperture combined with a metal-insulator-metal structure. *Opt Lett* **44**, 783–786 (2019).
39. Zheng J, Chen WD, Liu XC, Huang YR, Liu YY et al. Forming sub-45-nm high-aspect circle-symmetric spots with double bowtie aperture combined with metal-insulator-metal structure. *Appl Surf Sci* **447**, 300–306 (2018).
40. Huang YR, Liu L, Wang CT, Chen WD, Liu YY et al. Plasmonic direct writing lithography with a macroscopical contact probe. *Appl Surf Sci* **441**, 99–104 (2018).
41. Luo HW, Qin J, Kinzel E, Wang L. Deep plasmonic direct writing lithography with ENZ metamaterials and nanoantenna. *Nanotechnology* **30**, 425303 (2019).
42. Chang SW, Ni CYA, Chuang SL. Theory for bowtie plasmonic nanolasers. *Opt Express* **16**, 10580–10595 (2008).
43. Kinkhabwala A, Yu ZF, Fan SH, Avlasevich Y, Müllen K et al. Large single-molecule fluorescence enhancements produced by a bowtie nanoantenna. *Nat Photonics* **3**, 654–657 (2009).
44. Wang T, Li P, Chigrin DN, Giles AJ, Bezares FJ et al. Phonon-Polaritonic Bowtie Nanoantennas: Controlling Infrared Thermal Radiation at the Nanoscale. *ACS Photonics* **4**, 1753–1760 (2017).
45. Ma P, Salamin Y, Baeuerle B, Josten A, Heni W et al. Plasmonically enhanced graphene photodetector featuring 100 Gbit/s data reception, high responsivity, and compact size. *ACS Photonics* **6**, 154–161 (2019).
46. Kern J, Kullock R, Prangsma J, Emmerling M, Kamp M et al. Electrically driven optical antennas. *Nat Photonics* **9**, 582–586 (2015).
47. Du W, Wang T, Chu HS, Nijhuis CA. Highly efficient on-chip direct electronic –plasmonic transducers. *Nat Photonics* **11**, 623–627 (2017).
48. Qian HL, Hsu SW, Gurunatha K, Riley CT, Zhao J et al. Efficient light generation from enhanced inelastic electron tunnelling. *Nat Photonics* **12**, 485–488 (2018).
49. Zhang C, Hugonin JP, Coutrot AL, Sauvan C, Marquier F et al. Antenna surface plasmon emission by inelastic tunneling. *Nat Commun* **10**, 4949 (2019).
50. Lambe J, McCarthy SL. Light emission from inelastic electron tunneling. *Phys Rev Lett* **37**, 923–925 (1976).
51. Coombs JH, Gimzewski JK, Reihl B, Sass JK, Schlittler RR. Photon emission experiments with the scanning tunnelling microscope. *J Microsc* **152**, 325–336 (1988).
52. Aizpurua J, Apell SP, Berndt R. Role of tip shape in light emission from the scanning tunneling microscope. *Phys Rev B* **62**, 2065–2073 (2000).
53. Johansson P, Monreal R, Apell P. Theory for light emission from a scanning tunneling microscope. *Phys Rev B* **42**, 9210–9213 (1990).
54. Song H, Reed MA, Lee T. Single molecule electronic devices. *Adv Mater* **23**, 1583–1608 (2011).
55. Cazier N, Buret M, Uskov AV, Markey L, Arocas J et al. Electrical excitation of waveguided surface plasmons by a light-emitting tunneling optical gap antenna. *Opt Express* **24**, 3873–3884 (2016).
56. Landauer R, Martin T. Barrier interaction time in tunneling. *Rev Mod Phys* **66**, 217–228 (1994).
57. Shafir D, Soifer H, Bruner BD, Dagan M, Mairesse Y et al. Resolving the time when an electron exits a tunnelling barrier. *Nature* **485**, 343–346 (2012).
58. Kirtley JR, Theis TN, Tsang JC, Dimaria DJ. Hot-electron picture of light emission from tunnel junctions. *Phys Rev B* **27**, 4601–4611 (1983).
59. Parzefall M, Novotny L. Optical antennas driven by quantum tunneling: a key issues review. *Rep Prog Phys* **82**, 112401 (2019).
60. Novotny L, Hecht B. *Principles of Nano-Optics* 2nd ed (Cambridge University Press, Cambridge, 2012).
61. Simeone D, Esposito M, Scuderi M, Calafiore G, Palermo G et al. Tailoring electromagnetic hot spots toward visible frequencies in ultra-narrow gap Al/Al_2O_3 bowtie nanoantennas. *ACS Photonics* **5**, 3399–3407 (2018).
62. Ho PS, Kwok T. Electromigration in metals. *Rep Prog Phys* **52**, 301–348 (1989).
63. Liang WJ, Shores MP, Bockrath M, Long JR, Park H. Kondo resonance in a single-molecule transistor. *Nature* **417**, 725–729 (2002).
64. Liu YJ, Jiang ZJ, Qin J, Wang L. Localized surface plasmon mode-enhanced spectrum-tunable radiation in electrically driven plasmonic antennas. *Opt Lett* **45**, 5506–5509 (2020).
65. Ohnishi H, Kondo Y, Takayanagi K. Quantized conductance through individual rows of suspended gold atoms. *Nature* **395**, 780–783 (1998).
66. Purcell EM, Torrey HC, Pound RV. Resonance absorption by nuclear magnetic moments in a solid. *Phys Rev* **69**, 37–38 (1946).
67. De Vega S, De Abajo FJG. Plasmon generation through electron tunneling in graphene. *ACS Photonics* **4**, 2367–2375 (2017).
68. Parzefall M, Bharadwaj P, Jain A, Taniguchi T, Watanabe K et al. Antenna-coupled photon emission from hexagonal boron nitride tunnel junctions. *Nat Nanotechnol* **10**, 1058–1063 (2015).
69. Gurunarayanan SP, Verellen N, Zharinov VS, Shirley FJ,

Moshchalkov VV et al. Electrically driven unidirectional optical nanoantennas. *Nano Lett* **17**, 7433–7439 (2017).
70. Kullock R, Ochs M, Grimm P, Emmerling M, Hecht B. Electrically-driven Yagi-Uda antennas for light. *Nat Commun* **11**, 115 (2020).
71. Jiang ZJ, Wang L. Unidirectional propagation of electrically driven surface plasmon polaritons: a numerical study. *Nanotechnology* **31**, 455207 (2020).
72. Prangsma JC, Kern J, Knapp AG, Grossmann S, Emmerling M et al. Electrically connected resonant optical antennas. *Nano Lett* **12**, 3915–3919 (2012).

Acknowledgements

This work is supported by National Key Research and Development Program of China (2018YFB2200900), the Key R&D Program of Anhui (Grant No. 202004A05020077) and National Natural Science Foundation of China (61775206). The nanofabrication was carried out at the USTC Center for Micro and Nanoscale Research and Fabrication. We also thank Prof. Xianfan Xu of Purdue University for his warm-hearted discussion.

Competing interests

The authors declare no competing financial interests.